Journal of Nano- and Electronic Physics
Vol. **17** No 5, 05019(10pp) (2025)

Журнал нано- та електронної фізики
Том **17** № 5, 05019(10cc) (2025)

OPEN ACCESS

REGULAR ARTICLE

Effect of Ultrasonic Nanocrystal Surface Modification on Microhardness and Tensile Properties of Laser Powder Bed Fusion 316L Steel

B.V. Efremenko[1,*], Yu.G. Chabak[1,2], A. Amanov[3], V.G. Efremenko[1,2], O. Milkovič[2,4], E.V. Tsvetkova[1], I.M. Olejnik[1], A.V. Dzherenova[1]

[1] *Pryazovskyi State Technical University, 49044 Dnipro, Ukraine*
[2] *Institute of Materials Research, Slovak Academy of Sciences, 04001 Kosice, Slovakia*
[3] *Tampere University, Tampere, Finland*
[4] *Institute of Experimental Physics, Slovak Academy of Sciences, 04001 Kosice, Slovakia*

(Received 20 August 2025; revised manuscript received 21 October 2025; published online 30 October 2025)

Laser Powder Bed Fusion (LPBF) enables the fabrication of complex 316L stainless steel components, valued for their corrosion resistance and mechanical properties in aerospace, biomedical, and other sectors. However, LPBF 316L steel exhibits surface imperfections, limiting its high-demand applications. This study investigates the effects of Ultrasonic Nanocrystal Surface Modification (UNSM), an impact-based severe plastic deformation technique, on the microstructure, microhardness, and tensile properties of LPBF-manufactured 316L steel. Both as-built and post-LPBF annealed 316L samples were subjected to UNSM using a static load of 30 N, a frequency of 20 kHz, and a vibration amplitude of 30 μm. UNSM leads to texturing of the as-built cellular structure, accompanied by crystalline refinement, lattice defect accumulation, and deformation-induced martensite transformation, resulting in a surface hardness of 500-550 HV10. However, UNSM only slightly improves tensile strength while substantially reducing ductility due to intense work hardening and earlier surface cracking under tensile testing. Post-UNSM recrystallization annealing (at 900°C for 1 hour) promotes the formation of an ultrafine-grained microstructure (1-5 μm, average grain size 2.48 μm) in the near-surface layer affected by UNSM. This treatment restores ductility (total elongation of 61-63%) while maintaining elevated surface hardness (~400 HV10). For as-built specimens, the combination of UNSM and recrystallization annealing results in a superior strength-ductility balance, as reflected by an increased product of strength and elongation (PSE index), thereby enhancing both surface integrity and mechanical performance. In softer post-LPBF annealed samples, UNSM leads to deeper plastic deformation and a less steep hardness gradient. However, it also induces surface cracking, indicating the need for further optimization of UNSM parameters to accommodate the initial material hardness.

Keywords: 316L steel, Laser powder bed fusion, Ultrasonic nanocrystal surface modification, Microstructure, Micro-hardness, Tensile properties

DOI: 10.21272/jnep.17(5).05019 PACS numbers: 62.20.Qp, 62.25.Mn, 62.20.F–, 81.40.Ef

1. INTRODUCTION

Laser Powder Bed Fusion (LPBF), an advanced additive manufacturing technique, enables the precise fabrication of metallic components with complex geometries. Its layer-by-layer processing of metal powders not only enhances design flexibility but also contributes to cost reduction and efficient material utilization [1]. 316L austenitic stainless steel is one of the most widely used alloys in LPBF due to its superior corrosion resistance, favourable mechanical performance, and proven compatibility with demanding environments in aerospace, biomedical, chemical, and energy sectors [2]. However, the lower inherent strength and wear resistance of 316L steel limit its suitability for certain high-demand engineering applications. Furthermore, LPBF-fabricated 316L steel often exhibits surface imperfections, such as roughness and residual stresses, which can adversely affect its mechanical properties, limiting its performance in demanding environments [3]. To address these challenges, post-processing techniques, such as thermochemical treatment [4], surface severe plastic deformation (S²PD) [5], hardfacing [6], and plasma coating deposition [7, 8], are applied to 316L steel to enhance its surface integrity and mechanical strength.

Among these techniques, ultrasonic nanocrystal surface modification (UNSM) has emerged as a promising method to enhance surface integrity and mechanical properties [9]. UNSM is an impact-based S²PD method that employs high-frequency ultrasonic vibrations to

* vgefremenko@gmail.com

© 2025 The Author(s). Journal of Nano- and Electronic Physics published by Sumy State University. This article is distributed under the terms and conditions of the Creative Commons Attribution (CC BY) license.

Cite this article as: B.V. Efremenko et al., *J. Nano- Electron. Phys.* 17 No 5, 05019 (2025) https://doi.org/10.21272/jnep.17(5).05019

induce grain refinement and compressive residual stresses in the material's surface layer [10]. Unlike traditional surface treatments, UNSM offers precise control over deformation depth and is particularly effective for complex geometries produced by LPBF. This process significantly refines the microstructure (to grains smaller than 100 nm in diameter), reduces surface roughness, and enhances fatigue resistance, hardness, and tribological properties [9, 10]. Recent studies have demonstrated its effectiveness in improving the mechanical performance of Ti-6Al-4V [11], S45C steel [12], and other alloys, including LPBF 316L stainless steel [13-15]. Kim et al. [16] reported that the effect of UNSM treatment on the corrosion resistance of 316L depends on its sensitization level and can be either positive or negative. In most studies focusing on the effect of UNSM on LPBF 316L steel's performance, surface hardness and wear behaviour are primarily considered [13-15], while other properties, such as tensile behaviour, remain less explored. Furthermore, other aspects, such as the application of post-UNSM recrystallization annealing for tailoring 316L properties, have not been studied. At the same time, a deeper understanding of the interplay between UNSM parameters, post-treatment conditions, and the specific microstructural characteristics of LPBF 316L steel is critical for optimizing its mechanical behaviour.

The present research addresses the aforementioned gap in the literature by analysing the influence of ultrasonic nanocrystal surface modification on the tensile strength and ductility of LPBF 316L stainless steel through surface nanostructuring. By examining the correlations between UNSM, microstructure, and tensile properties, this study aims to advance post-processing approaches for additively manufactured 316L components, enabling their broader adoption in high-performance applications.

2. MATERIALS AND METHODS

316L stainless steel test specimens were additively manufactured via Laser Powder Bed Fusion using an Alfa-150D 3D-printing system (Additive Laser Technology, Dnipro, Ukraine). The starting material consisted of gas-atomized 316L stainless steel powder with a particle size distribution of 15-45 μm. The fabrication parameters were as follows: laser power of 195 W, scan velocity of 1150 mm/s, beam diameter of 45 μm, layer thickness of 40 μm, hatch spacing of 100 μm, stripe-based scanning strategy, and a 67° rotation angle between successive layers. The chemical composition of the fabricated samples was as follows: 0.022 wt.% C, 16.39 wt.% Cr, 11.92 wt.% Ni, 2.36 wt.% Mo, 0.80 wt.% Si, 1.08 wt.% Mn, 0.007 wt.% S, 0.018 wt.% P, with Fe as the balance.

Tensile test specimens were produced in a 4 mm-thick dog-bone configuration, with dimensions detailed in Fig. 1a. During manufacturing, the specimens were oriented parallel to the vertical (*Z*) build axis.

The samples were investigated under various conditions: (a) in their initial as-built state (designated AsB); (b) after post-LPBF annealing at 900 °C (designated A900); (c) following UNSM processing (labelled AsB/UNSM and A900/UNSM, respectively); and (d) after post-UNSM recrystallization annealing (marked AsB/UNSM/R and A900/UNSM/R, respectively). Heat treatments – both post-LPBF and post-UNSM – were conducted at 900°C in an electric muffle furnace under a protective atmosphere of technical-grade nitrogen (99.9% purity). The durations were 5 hours for post-LPBF annealing and 1 hour for post-UNSM annealing, followed by water quenching.

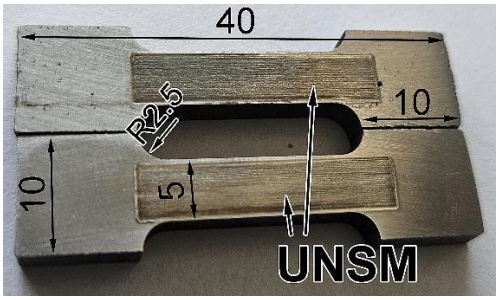

a

b

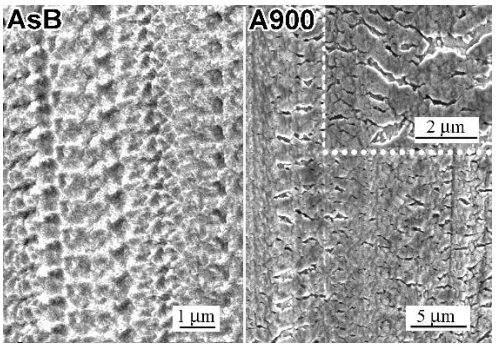

c

Fig. 1 – (a) View of the LPBF 316L specimens subjected to the UNSM treatment, (b) the trajectory of the UNSM treatment, (c) topography of UNSM-treated surfaces (left: AsB specimen; right: A900 specimen)

Ultrasonic Nanocrystal Surface Modification (UNSM) was performed on tensile specimens using equipment from «Design Mecha», as described in [13]. Prior to UNSM, sample surfaces were polished to a roughness of $Ra = 0.2$ μm to eliminate LPBF-induced surface irregularities and oxide layers. Both opposing surfaces of each specimen were treated, as illustrated in Fig. 1a. The UNSM parameters were as follows: static load of 30 N,

frequency of 20 kHz, processing speed of 2000 mm/min, vibration amplitude of 30 μm, 70 μm spacing between forward and backward tip movements, and a single scanning pass using a 2.38 mm diameter tungsten carbide (WC) ball tip. During processing, airflow was directed to the contact area to remove debris and prevent localized overheating. The UNSM scanning trajectory is shown in Fig. 1b. Following treatment, characteristic micro-indentations remained on the sample surfaces. In A900 specimens, indentation formation was accompanied by microcracks up to 0.5 μm in width, oriented perpendicular to the processing direction (Fig. 1c, right). In contrast, no such cracks were observed in AsB specimens (Fig. 1c, left).

Tensile testing was conducted using an electromechanical testing machine (TiraTest 2300, TIRA) at a loading speed of 1.5 mm/min. The following mechanical properties were derived: yield tensile strength (YTS), ultimate tensile strength (UTS), total elongation after fracture (TEL), and area reduction (AR). Microhardness measurements were performed using an LM700AT (LECO) tester with a 0.010 kg load. Microstructural analysis was carried out using optical microscopy (GX71, OLYMPUS) and scanning electron microscopy (JSM-7000F, JEOL) equipped with an INCAx-sight energy-dispersive spectroscopy (EDS) analyser (Oxford Instruments).

X-ray microdiffraction was performed in Bragg-Brentano reflective mode using a Rigaku Rapid D/MAX II diffractometer equipped with a molybdenum lamp and a curved detector. The incident beam was collimated to 0.3 mm and fixed at an incidence angle of 20°. Diffraction patterns were recorded over 15 minutes while rotating the sample along the φ-axis. The azimuthally integrated diffraction profiles are presented in the results section.

3. RESULTS

3.1 Microstructure Characterization

Fig. 2a illustrates the microstructure of the as-built 316L steel, which consists of rows of "melt pools" formed by laser melt scanning and localized powder melting/crystallization. As shown on the left side of Fig. 2a, the melt pools are oriented at an angle of 67°. These pools exhibit a complex intrinsic cellular microstructure composed of bundles of columnar crystals with varying lengths and cross-sectional dimensions (right side of Fig. 2a). The cellular structure is clearly visible in the SEM images (Fig. 2b). Depending on the spatial orientation of each bundle, its cross-section may appear as either equiaxed or elongated cells. The cross-sectional size of the cells varies by nearly an order of magnitude, ranging from 0.2 to 1.2 μm (Fig. 2b).

The cell boundaries consist of dislocation clusters [17] enriched with Mo, Ni, and Si relative to the cell interior, as confirmed by EDX profiling of Mo and Ni distribution (Fig. 2c). Point EDX analysis revealed that the cell interior contains 2.29 wt% Mo, 8.28 wt% Ni, and 0.60 wt% Si, while the cell boundaries exhibit 1.5-2 times higher concentrations: 4.54 wt% Mo, 12.84 wt% Ni, and 1.32 wt% Si, as shown in the EDX spectra in Fig. 2d.

In the post-LPBF annealed sample (A900), the overall microstructural pattern was preserved; however, SEM observations at higher magnification revealed complete degradation of the cellular structure (Fig. 2e). Instead, the A900 sample exhibits large, cell-free grains containing triangular etch pits (right side of Fig. 2e).

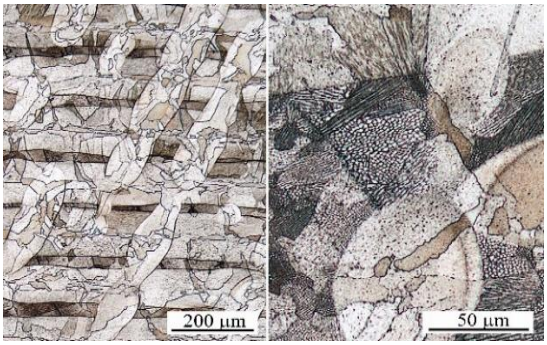

a

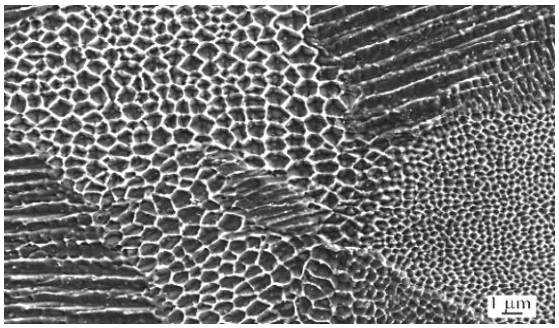

b

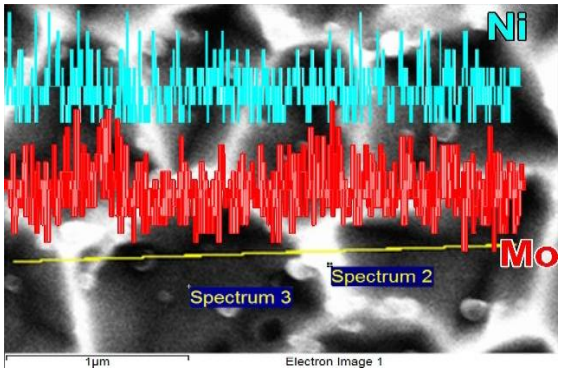

c

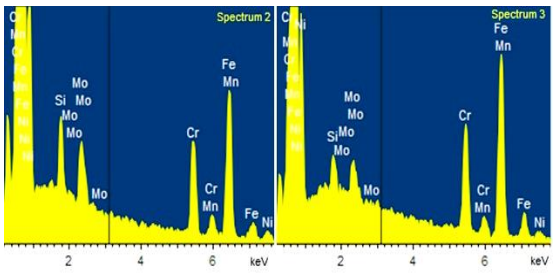

d

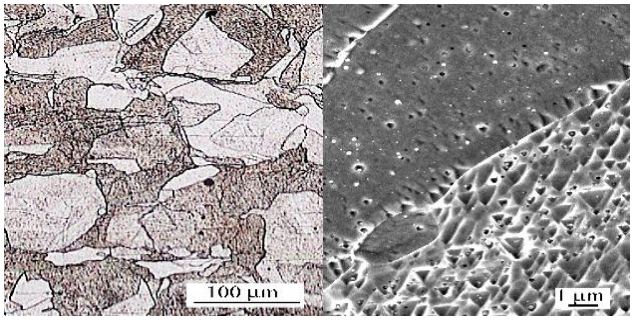

e

Fig. 2 – Microstructure of as-built LPBS 316L steel: (a) total view, (b) cellular pattern, (c) Mo and Ni distribution within cells, (d) EDX spectra of the cell boundary (Spectrum 2, left) and cell interior (Spectrum 3, right), (e) microstructure of the A900 specimen (left: grain pattern, right: etch pits)

The number of etch pits varies markedly between neighbouring grains, resulting in differences in coloration, as observed in optical micrographs (left side of Fig. 2e).

UNSM treatment induced deformation in the subsurface layers of the specimens, as evidenced by numerous dislocations slip bands extending to depths of 320 μm in the AsB/UNSM sample and 350 μm in the A900/UNSM sample (Fig. 3a and 3b, left). Near the surface, signs of metal flow were observed, manifested as bending of columnar crystals in the AsB/UNSM sample (Fig. 3a, right) and fiber-like structures in the A900/UNSM sample (Fig. 3b, right), extending to depths of approximately 10 μm and 25 μm, respectively.

Post-UNSM heat treatment (annealing at 900°C) induced recrystallization within the work-hardened layers. This is evidenced by the formation of fine recrystallized grains in the near-surface region, extending to a depth of approximately 120 μm in both the AsB/UNSM/R and A900/UNSM/R specimens, as delineated by the dotted line in Figs. 4a and 4c.

At the surface, the grains were the smallest (1-5 μm, average 2.48 μm), increasing to 15-20 μm at the boundary between the recrystallized and original structures (Fig. 4b, 4d, left). A distinctive feature of the recrystallized grains was the absence of etch pits,

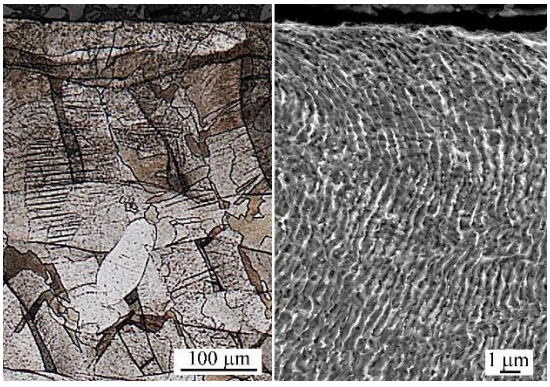

a

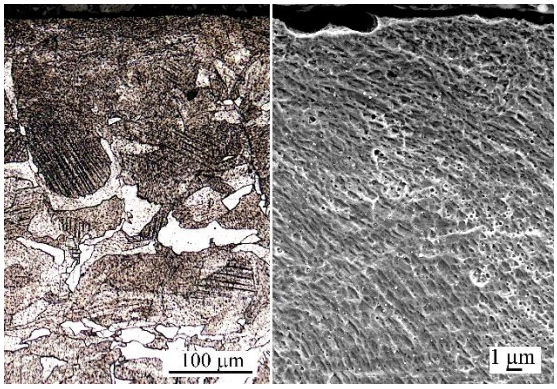

b

Fig. 3 – Cross-sectional images of the specimens subjected to UNSM. Multiple slip bands and metal flow in surface layers: (a) AsB/UNSM, and (b) A900/UNSM

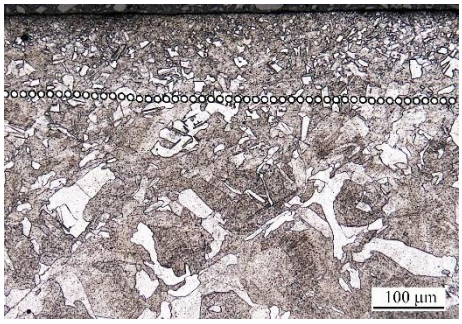

a

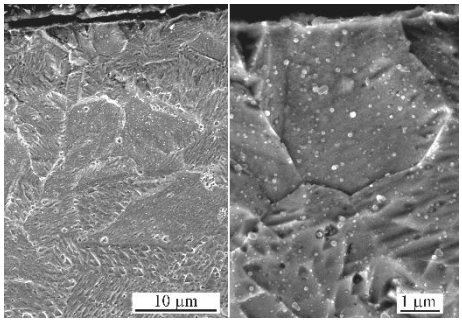

b

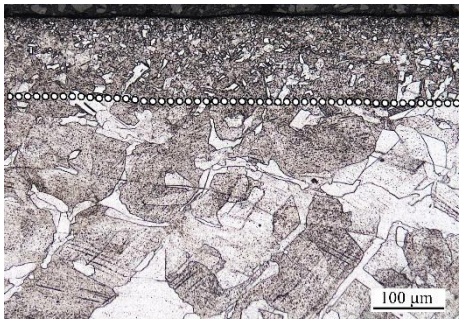

c

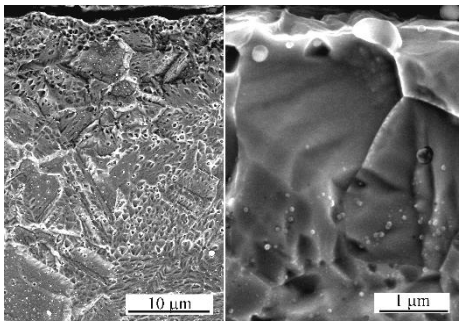

d

Fig. 4 – Cross-sectional images of the specimens subjected to UNSM followed by recrystallization annealing: (a) AsB/UNSM/R, and (b) A900/UNSM/R

indicating a reduced density of lattice defects (Fig. 4b, 4d, right). Notably, slip bands persisted in the larger grains beyond the recrystallized zone, suggesting that the degree of deformation in the deeper regions was insufficient to initiate recrystallization process.

3.2 XRD Study

The XRD results are shown in Fig. 5. As depicted in Fig. 5a, in the as-built state, LPBF 316L consists entirely of austenite (face-centred cubic (FCC) lattice), as evidenced by the distinct (111), (200), (220), and (311) peaks indicative of the γ-Fe phase.

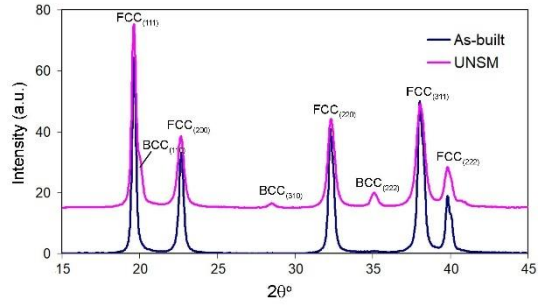

a

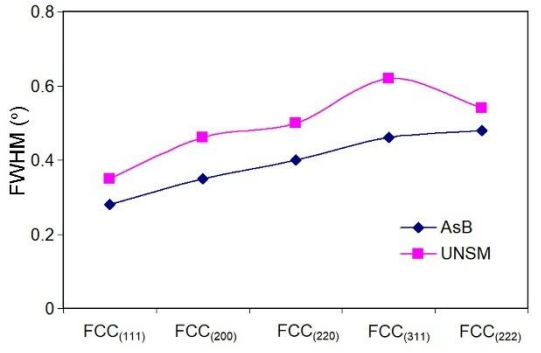

b

Fig. 5 – (a) The XRD patterns of the LPBF 316 steel for the AsB and UNSM samples. (b) FWHM values of the austenite peaks.

After UNSM treatment, the XRD pattern reveals significant structural changes. Specifically, minor diffraction peaks at (110), (310), and (222), corresponding to the α-Fe phase with a body-centred cubic (BCC) lattice, emerged. The volume ratio of FCC to BCC phases was calculated to be 95:5. Additionally, broadening of the FCC peaks was observed, as confirmed by the increased full width at half maximum (FWHM). As shown in Fig. 5b, the FWHM values for the UNSM-treated sample exceed those of the as-built specimen, indicating a higher density of crystalline imperfections [18], consistent with the intended effects of UNSM processing.

3.3 Microhardness Measurements

The cross-sectional microhardness profile is presented in Fig. 6. The results indicate that ultrasonic nanocrystalline surface modification substantially increased the hardness of the subsurface layers in both AsB and A900 specimens, establishing a hardness gradient that largely persisted following post-UNSM recrystallization annealing. In the AsB/UNSM sample, at depths of 10-30 μm, the microhardness reaches 500-550 HV_{10}, approximately 1.5 times higher than in the unhardened central layers (Fig. 6a). Between ~30 μm and 100 μm, the microhardness declines sharply, followed by a more gradual decrease, stabilizing at the baseline AsB level of 300-330 HV_{10} beyond ~300 μm depth. Post-UNSM annealing reduced the overall

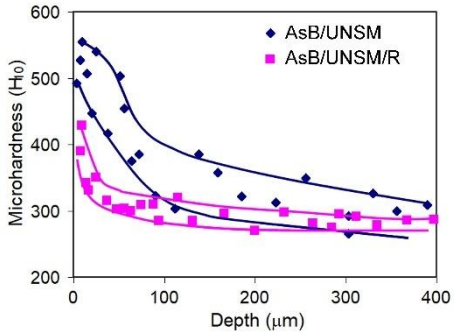

a

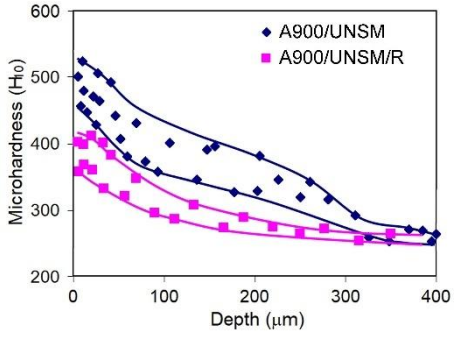

b

Fig. 6 – The microhardness profiles across the cross-section of the specimens (a) AsB/UNSM and AsB/UNSM/R; (b) A900/UNSM and A900/UNSM/R

hardness at all depths but preserved elevated hardness (390-430 HV_{10}) near the surface, up to a depth of 10-15 μm. In the AsB/UNSM/R sample, the hardness in the interior layers is 270-295 HV_{10}, lower than in the AsB/UNSM sample due to the annealing process.

In the A900/UNSM sample, surface modification resulted in a lower maximum hardness (450-525 HV_{10} near the surface); however, the microhardness profile is less steep compared to that of the AsB/UNSM sample, indicating more pronounced hardening in the deeper layers at depths of 100-300 μm. A similar trend is observed in the A900/UNSM/R specimen, where microhardness values exceed those of the AsB/UNSM/R sample up to a depth of 100 μm.

3.4 Tensile Properties Variation

The data presented in Fig. 7 illustrate the effects of UNSM and post-UNSM processing on the tensile properties and microhardness of LPBF 316L stainless steel. As shown in Fig. 7a, the as-built samples exhibit higher strength – YTS of 553 MPa and UTS of 664 MPa – exceeding that of conventionally manufactured 316L rolled steel. Furthermore, the as-built LPBF 316L steel demonstrates enhanced ductility, with a total elongation of 57% and an area reduction of 50% (Fig. 7b).

Ultrasonic nanocrystalline surface modification resulted in a modest increase (3-4%) in the strength characteristics of the as-built specimens, accompanied by a substantial decrease (22-26%) in ductility. In the A900 sample, UNSM led to a more pronounced increase in yield tensile strength – by 18% (up to 456 MPa) – but this improvement compromised ductility, which dropped to the level observed in the AsB/UNSM sample.

Fig. 7a also presents microhardness values measured on the UNSM-treated surface. Sample hardness varied proportionally with yield strength, peaking at 540 HV_{10} in the AsB/UNSM sample and reaching a minimum of 271 HV_{10} in the A900 sample. Surface hardness generally correlates with microhardness measured in the subsurface layers (Fig. 6).

Post-UNSM recrystallization annealing significantly enhanced the ductility of UNSM-processed samples, bringing both groups to similar higher levels (TEL of 61-63% and AR of 50-57%). Strength properties also equalized, decreasing to a yield tensile strength of 384-386 MPa and an ultimate tensile strength of 640 MPa. Notably, the reduction in strength during the recrystallization annealing was more pronounced for the AsB group samples compared to the A900 group.

The strength–ductility balance in structural steels is commonly assessed by the product of strength and elongation (PSE, defined as UTS × TEL, GPa×%) [19]). The evolution of PSE for the LPBF 316L specimens is presented in Fig. 7c. Given the minor differences in tensile strength across processing conditions, the change in PSE is primarily determined by the variation in TEL. Within the AsB group samples, the AsB/UNSM/R sample exhibits the highest PSE value, slightly surpassing the AsB sample.

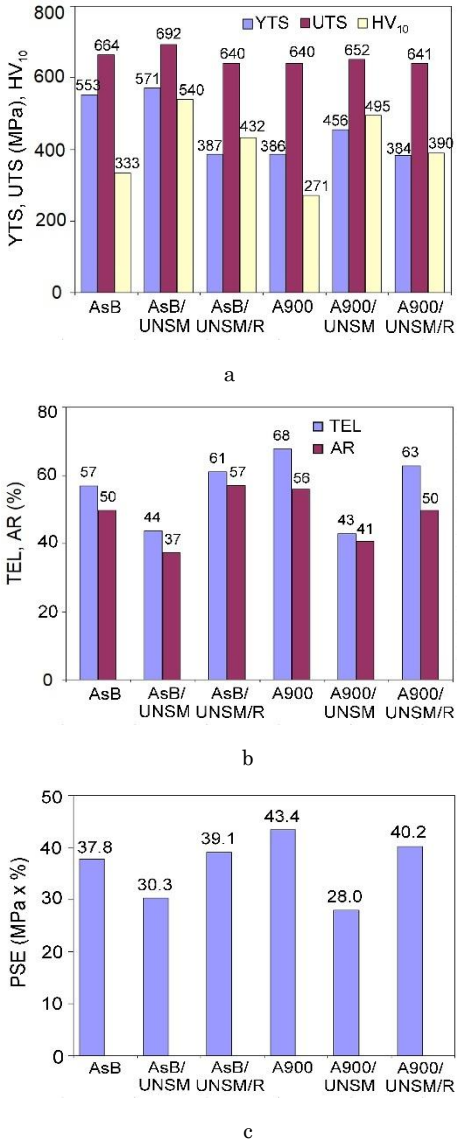

Fig. 7 – Tensile properties of the specimens studied: (a) YTS, UTS and microhardness, (b) TEL and AR, (c) PSE

In contrast, among the A900 group samples, the A900 outperforms the A900/UNSM/R sample, attaining the peak PSE value (43.4 GPa%). For both groups, the lowest PSE values correspond to UNSM-treated samples, attributed to their minimal ductility.

4. DUSCUSSION

Microstructure observations reveal that UNSM induces intense deformation of the as-built structure, causing bending of columnar crystals and texturing along the strain direction. Alongside these morphological changes, the intrinsic structure of the columnar grains is also modified. This is evident from significant work hardening and XRD peak broadening arising from the crystallite refinement and the development of microstrains, which may result from the accumulation of

lattice defects [18]. The XRD peak broadening (FWHM) enables estimation of crystallite size (D) and dislocation density using the Williamson-Hall method [20]:

$$\beta_{hkl}\cos\theta = \frac{k\lambda}{D} + 4\varepsilon\sin\theta \quad (1)$$

where β_{hkl}: the FWHM value, k: a shape factor (0.891), λ: the X-ray wavelength, θ: the Bragg angle, ε: the microstrain calculated as:

$$\varepsilon = \frac{\beta_{hkl}}{4\tan\theta}. \quad (2)$$

The average crystalline size can be found by Debye-Scherrer's equation [21]:

$$D = \frac{k\lambda}{\beta_{hkl}\cos\theta}. \quad (3)$$

The Williamson-Hall plot, constructed with "$4\sin(\theta)$" on the X-axis and "$\beta_{hkl}\times\cos(\theta)$" on the Y-axis (Fig. 8), was used to determine the experimental values of D and ε. The crystallite size was calculated from the Y-intercept of the linear fit to the data points, and the strain was obtained from the slope of the fit relative to the X-axis.

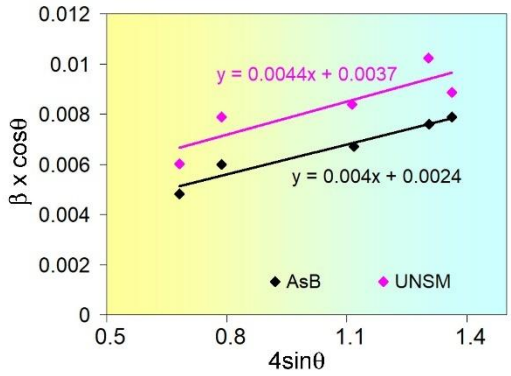

Fig. 8 – A Williamson-Hall plots for the specimens AsB and UNSM

The dislocation density (ρ_{XRD}) is calculated by the Williamson–Smallman equation [22]:

$$\rho_{XRD} = \frac{\sqrt{3K}\varepsilon}{Db}, \quad (4)$$

where b: the Burgers vector magnitude (taken as 2.58 Å for FCC lattice [23]), and K: parameter the elastic properties of the alloy and the dislocation disposition (taken as 1.2 [22]).

Using the Eqs. (3) and (4), the experimental D and ρ_{XRD} values were calculated as follows:

– for the AsB specimen: 60.4 nm and 4.87×10^{14} m^{-2}, correspondingly,

– for the UNSM specimen: 39.2 nm and 8.25×10^{14} m^{-2}, correspondingly.

Analysis of the data reveals that the structure of both samples can be characterized as nanoscaled, as the crystallite size (coherent scattering domains) is less than 100 nm. The nanoscale nature of as-built LPBF 316L steel arises from unique formation conditions and its distinct cellular morphology. UNSM provided additional refinement of crystallites, which is typical for this type of processing [13]. Furthermore, the as-built LPBF 316L sample exhibits a high dislocation density, which is attributed to the extensive boundaries of cellular structures formed by dislocation clots [17]. After UNSM, a 1.7-fold increase in lattice defect density was observed, resulting from the combined effect of dislocation gliding and pile-up interacting with the as-built cellular structure. The cell boundaries effectively obstruct dislocation movement, facilitating rapid defect accumulation. Consequently, this led to significant hardening of the samples, with the subsurface microhardness rising to 500-550 HV_{10}.

The emergence of BCC peaks in the XRD pattern of UNSM-treated sample indicates a deformation-induced martensite transformation γ-Fe → α′-Fe in LPBF 316L steel under the ultrasonic nano-modification. The formation of harder martensite further enhanced the hardness of 316L steel, consistent with findings in [24]. The probability of α′-martensite formation can be estimated based on the steel's chemical composition using the Angel equation [24]:

$$Md_{(30/50)}\ (^{o}C) = 413 - 13.7(\%Cr) - 9.5(\%Ni) - 8.1(\%Mn) - 18.5(\%Mo) - 9.2\ (\%Si) - 462\ (\%[C + N]) \quad (5)$$

where $Md_{(30/50)}$: the temperature at which 50% of the α′-martensite is formed under 30% tensile deformation.

Calculations reveal that the $Md_{(30/50)}$ temperature for the studied 316L steel is 5.3°C, whereas martensite formation upon cooling in this steel occurs only at cryogenic temperatures below –186°C [24]. Consequently, deformation-induced martensite formation in LPBF 316L is feasible, driven by the substantial plastic deformation from UNSM processing, which provides the energy required for the martensite transformation.

It is known that α′-martensite crystals tend to form in 316L steel, particularly at defect accumulation sites and near grain boundaries [25]. In LPBF 316L steel, the nucleation of α′-martensite is expected to be energetically favoured due to the presence of extensive cell boundaries composed of dislocation clusters. The stresses and stored energy associated with these dislocations contribute a driving force for the martensite transformation, supplementing the chemical driving force. However, the segregations of Mo, Ni, and Si atoms at cell boundaries (Fig. 2d) may inhibit martensite nucleation, as a $Md_{(30/50)}$ temperature drops to –48.6 °C in these areas. In contrast, nucleation within the cells may be facilitated ($Md_{(30/50)}$ = 43.0°C) due to the depletion in Mo, Ni, and Si. Presumably, the kinetics of deformation-induced martensite transformation in LPBF 316L steel are governed by the interplay of these factors.

The increased initial hardness of the AsB specimen led to localization of UNSM-induced deformation (hardening)

within a thin subsurface layer, thereby shielding the base material and limiting the inward transfer of strain (hardening). Due to the reduced hardening depth, macroplastic tensile deformation was initiated in the inner (non-hardened) layers at relatively low stress [26]. Consequently, the yield strength of the AsB/UNSM specimens increased only slightly compared to the AsB specimens, despite the enhanced surface hardness.

In contrast, the plasticity of the as-built specimens after UNSM treatment was significantly reduced (Fig. 7b). The hardened layer impeded metal flow in the inner (non-work-hardened) regions, resulting in elevated tensile stresses at the free surface. This led to multiple ruptures (indicated by double arrows in Fig. 9) and edge cracks (single arrow in Fig. 9) on the UNSM-treated surface. The propagation of these cracks caused premature failure of the specimens before the metal's ductility was fully exhausted.

Annealed A900 samples, characterized by lower yield strength, exhibited reduced resistance to deformation, resulting in severe strain and crack formation within the thin surface layer during UNSM (Fig. 1c). These cracks caused a sharp decline in ductility for the A900/UNSM specimens compared to their initial state (A900), with the effect being more pronounced than in the as-built (AsB) samples. However, the lower initial yield strength of A900 facilitated deeper deformation penetration during UNSM, as indicated by a less steep microhardness gradient relative to the AsB specimen. This deeper hardening contributed to a greater UNSM-induced increase in yield strength for the A900 specimens (+18%) compared to the AsB ones (+3%).

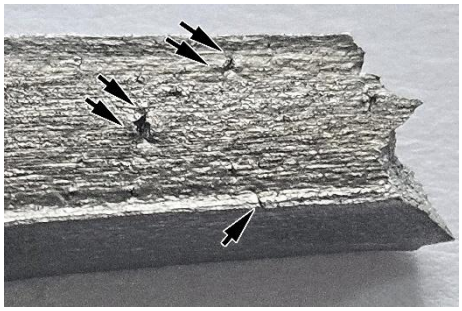

Fig. 9 – Cracks on the UNSM-treated surface of the AsB specimen appeared during tensile testing.

When evaluating the applicability of UNSM for processing LPBF 316L stainless steel, it is evident that UNSM effectively enhances surface hardness, which is advantageous for improving tribological performance and fatigue life [27]. In such applications, hardness serves as a more relevant indicator than yield strength, since YTS reflects resistance to macroplastic deformation throughout the entire sample volume rather than within the subsurface layers. However, under the applied processing regime, UNSM significantly reduces the ductility of LPBF 316L steel, which poses a limitation for components exposed to substantial tensile or bending loads during service.

For such applications, combining UNSM with subsequent recrystallization annealing, as applied in this study (900°C, 1 h), is more appropriate. In the case of UNSM+R, the strengthening effect of work hardening (associated with high dislocation density) is replaced by an alternative mechanism – grain boundary strengthening, the extent of which is quantified by the Hall–Petch relationship:

$$\Delta\sigma_Y = k_y \cdot d_G^{-0.5} \tag{6}$$

where d_G: a grain diameter, k_y: a material-dependant coefficient.

As shown in Fig. 4, an ultrafine-grained (UFG) structure [28], with a grain size ranging from 1 to 5 μm (average value: 2.53 μm), forms on the UNSM-treated surface following recrystallization annealing. According to [29], the Hall–Petch relationship for UFG 316L stainless steel can be expressed as follows:

$$\sigma_{YS} = 1033.4 + 82.8 \cdot d_G^{-0.5}. \tag{7}$$

By substituting the average grain size of the near-surface recrystallized layer (2.48 μm) into Eq. (7), the yield strength is calculated to be 1085.4 MPa. According to Pavlina and Van Tyne [30], the yield strength of steel with non-martensitic microstructures exhibits a linear correlation with its hardness (HV):

$$\text{YTS} = -90.7 + 2.65 \cdot \text{HV}. \tag{8}$$

Given the calculated yield strength of the recrystallized UFG structure (1085.4 MPa), its corresponding hardness is estimated at 409.6 HV. This value closely matches the hardness of the near-surface layer in the AsB/UNSM/R sample (Fig. 6a), highlighting the dominant role of grain refinement in enhancing hardness. Remarkably, a 30% increase in surface hardness is accompanied by improved ductility: following recrystallization annealing, the total elongation increased from 57% (AsB) to 61% (AsB/UNSM/R). As a result, the PSE index of the AsB/UNSM/R sample exceeds those of both AsB and AsB/UNSM, indicating a more balanced combination of strength and ductility. Therefore, combining UNSM with recrystallization annealing improves ductility, surface hardness, and structural integrity in LPBF 316L stainless steel.

UNSM is also effective in increasing the surface hardness of post-LPBF annealed samples (A900). However, due to the lower initial hardness of A900, UNSM treatment is accompanied by the formation of surface microcracks. Thus, the UNSM processing regime should be tailored to the steel's initial hardness to mitigate crack formation during treatment.

5. CONCLUSIONS

Ultrasonic Nanocrystal Surface Modification (UNSM), applied with a static load of 30 N, a frequency of 20 kHz, and a vibration amplitude of 30 μm, was performed on

LPBF-manufactured 316L stainless steel in both the as-built (AsB) and 900°C-annealed (A900) states. The study demonstrated that UNSM significantly enhanced the surface hardness of LPBF 316L stainless steel (up to 500-550 HV_{10}) due to nanostructuring, lattice defect accumulation, and deformation-induced γ-Fe → α′-Fe phase transition. However, UNSM only slightly increased the tensile strength (YTS and UTS) while notably reducing the ductility of AsB specimens, primarily due to intense surface work hardening and early crack formation on the treated surface. In A900 samples, the lower yield strength resulted in deeper plastic deformation and surface cracking during the UNSM process.

Post-UNSM recrystallization annealing (900°C for 1 hour) mitigated these drawbacks by forming an ultrafine-grained structure (grain size of 1-5 μm, average 2.48 μm) within the UNSM-modified layer. In AsB specimens, this approach improved ductility while maintaining elevated surface hardness (approximately 400 HV_{10}), resulting in a superior strength–ductility balance, as evidenced by the increased PSE index. Thus, UNSM followed by post-annealing optimizes LPBF 316L stainless steel for applications requiring both surface integrity and mechanical performance. The UNSM processing regime should be tailored to the initial hardness of LPBF 316L steel to prevent surface cracking during treatment.

ACKNOWLEDGMENTS

This research was funded by the Ministry of Education and Science of Ukraine (project No. 0123U101834).

REFERENCES

1. T. DebRoy, H.L. Wei, J.S. Zuback, T. Mukherjee, J.W. Elmer, J.O. Milewski, A.M. Beese, A. Wilson-Heid, A. De, W. Zhanget, *Prog. Mater. Sci.* **92**, 112 (2018).
2. R. Kocich, L. Kunčická, P. Minárik, *Mater. Des.* **253**, 113973 (2025).
3. B.V. Efremenko, V.I. Zurnadzhy, Yu.G. Chabak, V.G. Efremenko, K.V. Kudinova, V.A. Mazur, *Mater. Today: Proc.* **66**, 2587 (2022).
4. T.V. Loskutova, I.S. Pogrebova, V.G. Khyzhnyak, M.M. Bobina, N.S. Nikitina, *Mater. Today: Proc.* **6**, 202 (2019).
5. M.O. Vasylyev, B.M. Mordyuk, S.I. Sydorenko, S.M. Voloshko, A.P. Burmak, N.V. Franchik, *Metallofizika i Noveishie Tekhnologii* **39** No 7, 905 (2017).
6. B. Trembach, Y. Silchenko, O. Balenko, D. Hlachev, K. Kulahin, H. Heiko, O. Bellorin-Herrera, S. Khabosha, O. Zakovorotnyi, I. Trembach, *Int. J. Adv. Manuf. Technol.* **134**, 309 (2024).
7. V.G. Efremenko, K. Shimizu, T.V. Pastukhova, Yu.G. Chabak, K. Kusumoto, A.V. Efremenko, *J. Friction Wear* **38** No 1, 58 (2017).
8. O.V. Sukhova, *Probl. At. Sci. Technol.* **128** No 4, 77 (2020).
9. A. Kishore, M. John, A.M. Ralls, S.A. Jose, U.B. Kuruveri, P.L. Menezes, *Nanomaterials* **12** No 9, 1415 (2022).
10. A.K. Gujba, Z. Ren, Y. Dong, C. Ye, M. Medraj, *Surf. Coat. Technol.* **307**, 157 (2016).
11. H. Zhang, R. Chiang, H. Qin, Z. Ren, X. Hou, D. Lin, *Int. J. Fatigue* **103**, 136 (2017).
12. X. Cao, Y. Pyoun, R. Murakami, *Appl. Surf. Sci.* **256**, 6297 (2010).
13. A. Amanov, *Surf. Coat. Technol.* **398**, 126080 (2020).
14. Y. Zhang, L. Peng, Y. Wang, C. Ye, *Procedia CIRP* **123**, 481 (2024).
15. S.-Y. Cho, M.-S. Kim, Y.-S. Pyun, D.-S. Shim, *Metals* **11**, 843 (2021).
16. K.-T. Kim, J.-H. Lee, Y.-S. Kim, *Materials* **10**, 713 (2017).
17. Y.G. Chabak, B.V. Efremenko, V.I. Fedun, V.I. Zurnadzhy, V.I. Tyutyunnikov, A.V. Dzherenova, E.V. Tsvetkova, V.I. Zhuk, V.G. Efremenko, *Romanian Journal of Physics* **67**, 501 (2022).
18. T. Ungár, *Scripta Materialia* **51** No 8, 777 (2004).
19. F. Huang, Q. Chen, H. Ding, Y. Wang, X. Mou, *J. Chen. Materials* **27** No 14(5), 1121 (2021).
20. V. Mote, Y. Purushotham, B. Dole. *J. Theor. Appl. Phys.* **6**, 6 (2012).
21. M. Sivagami, I.V. Asharani, *Inorg. Chem. Commun.* **145**, 110054 (2022).
22. J. Gubicza, *Eur. Phys. J. Spec. Top.* **231**, 4153 (2022).
23. Y. Dong, Z. Sun, H. Xia, J. Feng, J. Du, W. Fang, B. Liu, G. Wang, L. Li, X. Zhang, *Metals* **8**, 742 (2018).
24. N. Solomon, I. Solomon, *Revista de Metalurgia* **46** No 2, 121 (2010).
25. S.M. Hasan, A. Ghosh, D. Chakrabarti, S.B. Singh, *Mater. Sci. Eng. A* **872**, 144930, (2023).
26. Z.A. Duriagina, M.R. Romanyshyn, V.V. Kulyk, T.M. Kovbasiuk, A.M. Trostianchyn, I.A. Lemishka, *J. Achiev. Mater. Manufact. Eng.* **100** No 2, 49 (2020).
27. V.G. Efremenko, Yu.G. Chabak, V.I. Fedun, K. Shimizu, T.V. Pastukhova, I. Petryshynets, A.M. Zusin, *Vacuum* **185**, 110031 (2021).
28. Yi Huang, T.G. Langdon, *Mater. Today* **16** No 3, 85 (2013).
29. H.E. Sabzi, E. Hernandez-Nava, X.-H. Li, H. Fu, D. San-Martín, P.E.J. Rivera-Díaz-del-Castillo, *Mater. Des.* **212**, 110246 (2021).
30. E. Pavlina, C. Van Tyne, *J. Mater. Eng. Perform.* **17**, 888 (2008).

Вплив ультразвукової нанокристалічної модифікації поверхні на мікротвердість та механічні властивості на розтяг сталі 316L, отриманої методом Laser Powder Bed Fusion

Б.В. Єфременко[1], Ю.Г. Чабак[1,2], А. Аманов[3], В.Г. Єфременко[1,2], О. Мілковіч[2,4], О.В. Цветкова[1], І.М. Олійник[1], А.В. Джеренова[1]

[1] *Приазовський державний технічний університет, 49044 Дніпро, Україна*
[2] *Інститут матеріалознавства Словацької Академії наук, 04001 Кошице, Словаччина*
[3] *Університет м. Тампере, 33720 Тампере, Фінляндія*
[4] *Інститут експериментальної фізики Словацької Академії наук, 04001 Кошице, Словаччина*

Технологія Laser Powder Bed Fusion (LPBF) дає можливості швидкого виготовлення компонентів складної форми із нержавіючої сталі 316L, яка відома своєю високими корозійною стійкістю і механічні властивості, завдяки чому широко використовується в високотехнологічних галузях промисловості. При виготовленні методом LPBF сталь 316L часто має поверхневі дефекти, що обмежує її застосування в умовах інтенсивного навантаження. В даній роботі досліджено вплив ультразвукової нанокристалі-чної модифікації поверхні (UNSM)) на мікроструктуру, мікротвердість і механічні властивості на роз-тяг LPBF сталі 316L. UNSM виконували на зразках як у вихідному (друкованому) стані, так і в відпа-леному при 900 °C стані. Застосовані параметри обробки: статичне навантаження – 30 Н, частота уда-рів – 20 кГц, амплітуда вібрації – 30 мкм. UNSM-обробка спричинила деформацію та текстурування стовпчастої структури друкованих зразків, що викликало подрібнення кристалітів, підвищення щіль-ності дефектів решітки та ініціювало деформаційне мартенситне перетворення аустеніту. Внаслідок цього поверхнева твердість зросла до 500-550 HV10, втім міцність на розтяг підвищилась незначно, а пластичність суттєво знизилась. Поєднання UNSM з рекристалізаційним відпалом (900 °C, 1 год) сприяло формуванню у деформованому шарі ультрадрібнозернистої (1-5 мкм) структури, що дозволило відновити пластичність сталі при збереженні підвищеного рівня поверхневої твердості (~ 400 HV10). Така комбінована обробка забезпечила оптимальний баланс між міцністю та пластичністю, що підтве-рджується зростанням індексу PSE порівняно з необробленим матеріалом. У більш м'яких (відпале-них) зразках, UNSM забезпечила глибшу деформацію та менш виражений градієнт твердості, однак спричинила появу поверхневих мікротріщин. Це свідчить про необхідність коригування режимів UNSM відносно вихідної твердості зразків для запобігання утворенню тріщин впродовж обробки.

Ключові слова: Сталь 316L, Laser Powder Bed Fusion, UNSM, Мікроструктура, Мікротвердість, Властивості при випробуваннях на розтяг.